Article:
Zoura, D orcid.org/0000-0001-9645-7803, Hill, DJ orcid.org/0000-0001-5492-3925, Dolan, AM orcid.org/0000-0002-9585-9648 et al. (3 more authors) (2019) Atmospheric carbon dioxide, ice sheet and topographic constraints on palaeo moisture availability in Asia. Earth and Planetary Science Letters, 519. pp. 12-27. ISSN 0012-821X

https://doi.org/10.1016/j.epsl.2019.04.035

Atmospheric carbon dioxide, ice sheet and topographic constraints on palaeo moisture availability in Asia

D. Zoura[a], D.J. Hill[a], A.M. Dolan[a], S.J. Hunter[a], Z. Tang[b], A.M. Haywood[a]

[a] School of Earth and Environment, University of Leeds, Leeds LS2 9JT, UK

[b] Key Laboratory of Cenozoic Geology and Environment, Institute of Geology and Geophysics, Chinese Academy of Sciences, Beijing 100029, China

Abstract

Today, the hydrological regime in East and South Asia is dominated by the monsoons, whilst central Asia is characterized as arid. Studies that have examined the onset of aridity and the intensification of the monsoons in Asia have generated significant debate, especially in respect to the timing of monsoon onset and how this relates to the potential causal mechanisms. The uplift of the Tibetan Plateau, the retreat of the Paratethys Sea, and the global cooling after the Eocene/Oligocene transition are all considered major drivers of Asian aridity and monsoonal intensification. However, little is known about each of these factor's contribution to the development of modern monsoon behaviour. Here, for the first time, we perform sensitivity simulations of a fully coupled ocean-atmosphere climate model (HadCM3) to investigate the effect of the Greenland and Antarctic ice-sheets formation, atmospheric carbon dioxide (CO_2) variability, and Tibetan Plateau uplift on East Central Asian aridity and monsoon driven precipitation. We focus on three individual regions, the South Asian Monsoon, the East Asian Monsoon and the Arid East Central Asia and we present the annual precipitation cycle and the moisture availability over each region. Our results show that of the parameters investigated the primary control on Asian hydroclimate is the topography of the Tibetan Plateau. Furthermore, our results highlight that the significance of each forcing depends on the component of the hydrological region and factors studied, a factor that proxy interpretation need to take into consideration.

Keywords: monsoons, Eurasia, climate, aridity, GCM, proxies

1. Introduction

Climate change is implicated in the spread of arid areas in Central Asia over the last 50 million years and is considered as potentially one of the major drivers for the progressive desertification of China being experienced today (Wang and Chen, 2013). However, the exact timing and mechanisms associated with the onset of Asian aridity and subsequent intensification is debated with some research placing it prior to mid-Miocene (Zhuang et al., 2011), early Miocene (Guo et al., 2002) and even the Eocene to Oligocene Transition (EOT) (e.g. Dupont-Nivet et al., 2007). Previous work on the Cenozoic aridification of Central Asia has highlighted the importance of Himalayan and Tibetan Plateau uplift, the Paratethys Sea retreat and the global cooling, potentially linked to atmospheric CO_2 decline, after the EOT (Jian et al., 2014). However, the contribution of each of these factors to the intensification of aridity remains unclear.

The Tibetan Plateau (TP) uplift was the most dramatic tectonic event in recent geological history, and has been considered as an important driving force for the Earth's climate and environmental change. The TP serves as a major topographic barrier to atmospheric flow (Liu and Dong, 2013). The TP uplift is suspected as a trigger of the Indian monsoon by providing a topographical high that opposes the classical Hadley circulation (Molnar et al., 1993), while geological evidence links it with the development of the Asian monsoon and inland aridification (Liu and Dong, 2013). However, the contribution made by the long-term uplift of the TP to inland aridification is only partially known. Climate model simulations show that the TP was the major mechanism driving shifts in atmospheric circulation, while at the same time forming a southern orographic barrier to inland Asia moisture supply (DeCelles et al., 2007; Zhuang et al., 2011). Additionally, Qian et al. (2011) suggests that the TP influences the South (SAM) and East (EAM) Asian monsoon through its dynamical and thermal forcing.

Antarctic ice sheet growth has been linked to EAM intensification through an increase of cross-equatorial SST and pressure gradients (Ao et al., 2016), and climate model studies suggest that associated global cooling is linked to a decrease in atmospheric CO_2 (e.g. Lefebvre et al., 2013).

Moreover, Hunter et al. (2013) noted changes in precipitation patterns under increasing levels of CO_2, and in turn CO_2 combined with changes in precipitation, have been a primary driver leading to regional changes in vegetation patterns (Khon et al., 2014).

Our understanding of the establishment, intensification and evolution of Asian aridity, and of the monsoonal intensification, remains incomplete for a variety of reasons. Firstly, the tectonics, uplift rates and palaeo-latitude estimates remain uncertain (i.e. during Oligocene, estimates on TP elevation presents differences of up to 2 km (Dupont-Nivet et al., 2008; Molnar et al., 2010; Rowley and Currie, 2006). Secondly, the interpretation of proxy data for Central Asia can be challenging due to the difference in scale of recorded variability for each proxy (i.e. lacustrine/marine sediments, terrestrial sediments, pollen). The sensitivity of proxy records to local climate and environmental factors also has to be taken into account in order to fully understand the contribution of each forcing. Additionally, even though previous climate modelling has studied the impact of the TP uplift and CO_2 change (An et al., 2001; Kutzbach and Liu, 1997), there has not been a systematic approach where the same model is used to study the relative contributions of the TP uplift and CO_2 increase together with the formation of the Antarctic and Greenland ice-sheets that was also formed after the EOT.

For the first time we perform a number of pre-industrial sensitivity experiments, with different CO_2, TP elevation and ice-sheet coverage as model boundary conditions. Focusing on aridity and monsoonal circulation we address the following questions: i) how is Asian aridity and the monsoons affected by changes in ice-sheet coverage? ii) Is Asian aridification and monsoonal intensification controlled by CO_2 decrease? iii) What is the impact of the Himalayan orogen and TP uplift on the established aridity in Central Asia and monsoonal circulation of the continent? iv) What is the relative contribution of each factor to climatic change in Asia?

2. Methods

2.1 Model description and evaluation

The General Circulation Model (GCM) used for this study is the UK Met Office coupled atmosphere-ocean HadCM3, using the MOSES 1 land-surface model (Cox et al., 1999). The HadCM3 model consists of a dynamically coupled atmosphere, ocean and sea-ice model (see Gordon et al., 2000 for further details). The horizontal resolution of the model is 3.75^{o} x 2.5^{o} for the atmosphere which corresponds to 278 km x 295 km at 45^{o} latitude and 278 x 417 km at the equator and 1.25^{o} x 1.25^{o} for the ocean. The atmosphere and ocean are represented by 19 and 20 vertical levels respectively. The Unified Model can produce precipitation from two schemes. Namely the convection scheme and the large scale precipitation scheme. The large-scale precipitation and cloud scheme is formulated in terms of an explicit cloud water variable following Smith (1990). HadCM3 has been used successfully in the representation of modern Asian climate as shown by Dabang et al. (2005) where the comparison between GCM outputs focused on the East Asian climate showed that HadCM3 can reproduce with success both annual and seasonal precipitation and surface air temperature. Furthermore, studies of precipitation and tropical Sea Surface Temperature (SST) for all four seasons yield a well-represented monsoon (Inness and Slingo, 2003; Turner et al., 2005). In conclusion, the HadCM3 model is an appropriate tool to study the Asian climate, especially in terms of precipitation (Lunt et al., 2010).

2.2 Boundary conditions and experimental design

Eight simulations have been performed in this study including a pre-industrial control experiment (Fig. 1c). Pre-industrial atmospheric CO_2 concentration levels for the control experiment (PreInd) were set to 280 ppmv. To assess Asia's hydrological sensitivity to rising CO_2 values two more simulations are performed with 2 x PreInd CO_2 and 4 x PreInd CO_2 values (2piCO2, 4piCO2). The selected atmospheric CO_2 values are within the suggested range during the EOT (450 – 1500 ppmv) (Pearson et al., 2009). 2piCO2 values are below the threshold for Antarctic glaciation (700 – 840 ppmv) (DeConto et al., 2008) and within the range of suggested values for Mid to Late Oligocene (Pagani et al., 2005), while 4piCO2 values are consistent with Early Oligocene values (Pearson et al., 2009). Asian climate response to ice-sheet coverage is explored through the NoGrIS and NoIce simulations (Fig. 1d), where the Greenland ice sheet and both the whole Antarctic and Greenland ice-sheets are removed respectively.

Furthermore, to investigate the effects of the TP uplift on the Asian climate alone, we changed the regional topography of the TP to flat (FlatTP) (Fig. 1b) and to an Oligocene-like TP topography (Fig.1e). The Oligocene-like topography used in this set of experiments, uses Oligocene palaeoelevation estimates derived from Markwick (2007) implemented over the area 62.5°E and 125°E and 20°N – 52.5°N. The Oligocene-like topography places the high-elevation TP at lower latitudes than present day, hence providing us with the opportunity to explore not only the response to elevation changes but also to the latitudinal distribution of high elevation topography. Finally, in the simulation called Combo we simulate a combination of the abovementioned changes in boundary conditions. Specifically, the TP topography is set to match the one of the Oligocene, CO_2 values are set to 2 x the PreInd level and there is no ice sheet coverage (Fig. 1c). All other boundary conditions, apart from those explicitly mentioned, are kept at pre-industrial values.

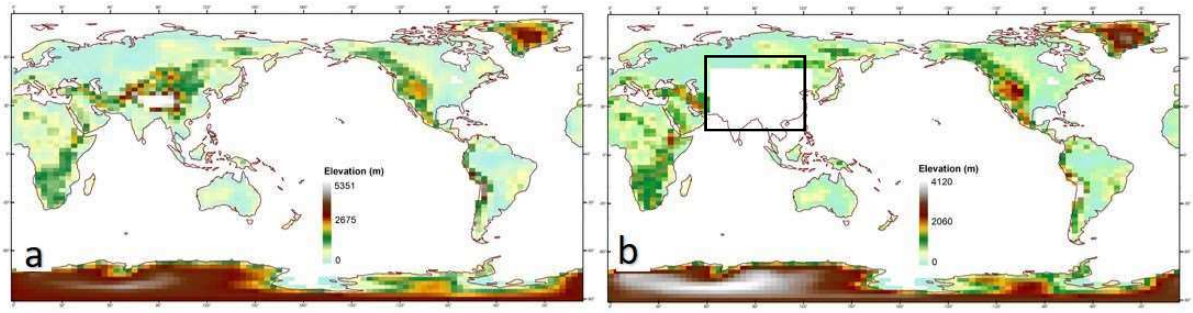

c

Experiment name	atm. CO_2	Topography	Greenland ice sheet	Antarctica ice sheet
PreInd	Pi (280 ppmv)	pi	modern extent	modern extent
2piCO2	2 x pi	pi	modern extent	modern extent
4piCO2	4 x pi	pi	modern extent	modern extent
NoGrIS	pi	pi	ice-free	modern extent
NoIce	pi	pi	ice-free	ice-free
FlatTP	pi	flat TP	modern extent	modern extent
OligTP	pi	Oligocene TP	modern extent	modern extent
Combo	2 x pi	Oligocene TP	ice-free	ice-free

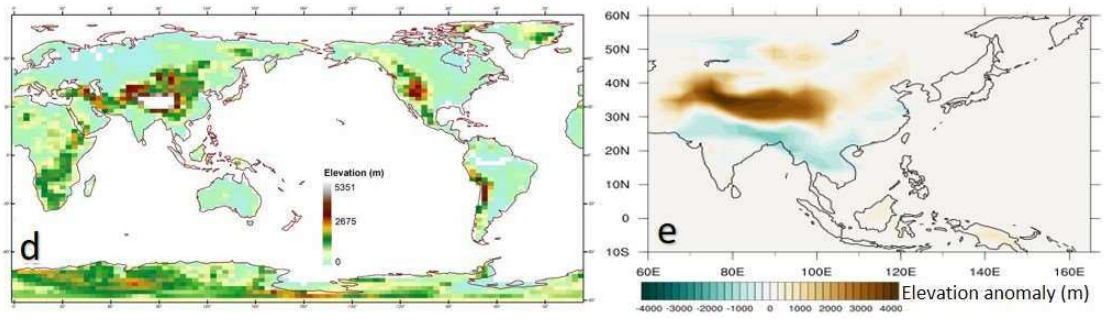

Fig. 1: Boundary conditions for the simulations in this study: a) Pre-industrial topography, b) Flat Tibetan Plateau (TP), d) No ice Greenland and Antarctic, e) Elevation anomaly between OligTP and PreInd experiments (PreInd – OligTP) (Elevation scales are common only for a and d), c) boundary conditions used for all the experiments.

2.3 Climatological variables and analysis techniques

When considering the sensitivity of the Asian climate to different forcings, it is important to be aware of the diversity of climates present in Asia. For example, the environmental conditions over South and East Asia are dominated by the monsoons, while Central Asia is characterized by arid conditions. Analysing variables over the whole of Asia can only provide a general view of the pattern and magnitude of change, but the underlying causalities and mechanisms cannot be easily understood without studying the three main monsoonal systems of Asia individually (Fig. 2j). The first step is to spatially define the monsoonal domain. In general, different studies have used different extents for the monsoon domain according to the variable they focus on. For example, Parthasarathy et al. (1994) used the seasonally averaged precipitation over only the Indian subcontinent to develop the All-Indian Summer Rainfall index. Webster and Yang (1992) studying the wind shear and the Outgoing Longwave Radiation (OLR) selected the domain from 0°-20° N, 40°-110° E. Wang et al. (2008) defined an East Asian – Western North Pacific index extending from 5° – 15° N, 90° – 130° E and from 20° – 30° N to 110° – 140° E. For the purposes of this study we focus on the monsoons over Asia during boreal summer. Namely we study the South Asian Monsoon (SAM) and the East Asian Monsoon (EAM) separately, as they differ in both climatology and variability (Cherchi et al., 2011). Using the domains as defined by Webster et al. (1998) and Wang (2005) for the SAM and EAM respectively, we averaged the monthly precipitation over these regions in an effort to not only assess the monsoonal change, but also the climate response over Asia under non-monsoonal circulation. Finally, in order to study the forcings that drive aridity over Central Asia we also analyse the same variables for the Arid East Central Asia (AECA) region located at 75° – 105° E, 35° – 55° N (Hong et al., 2014) (Fig. 2j).

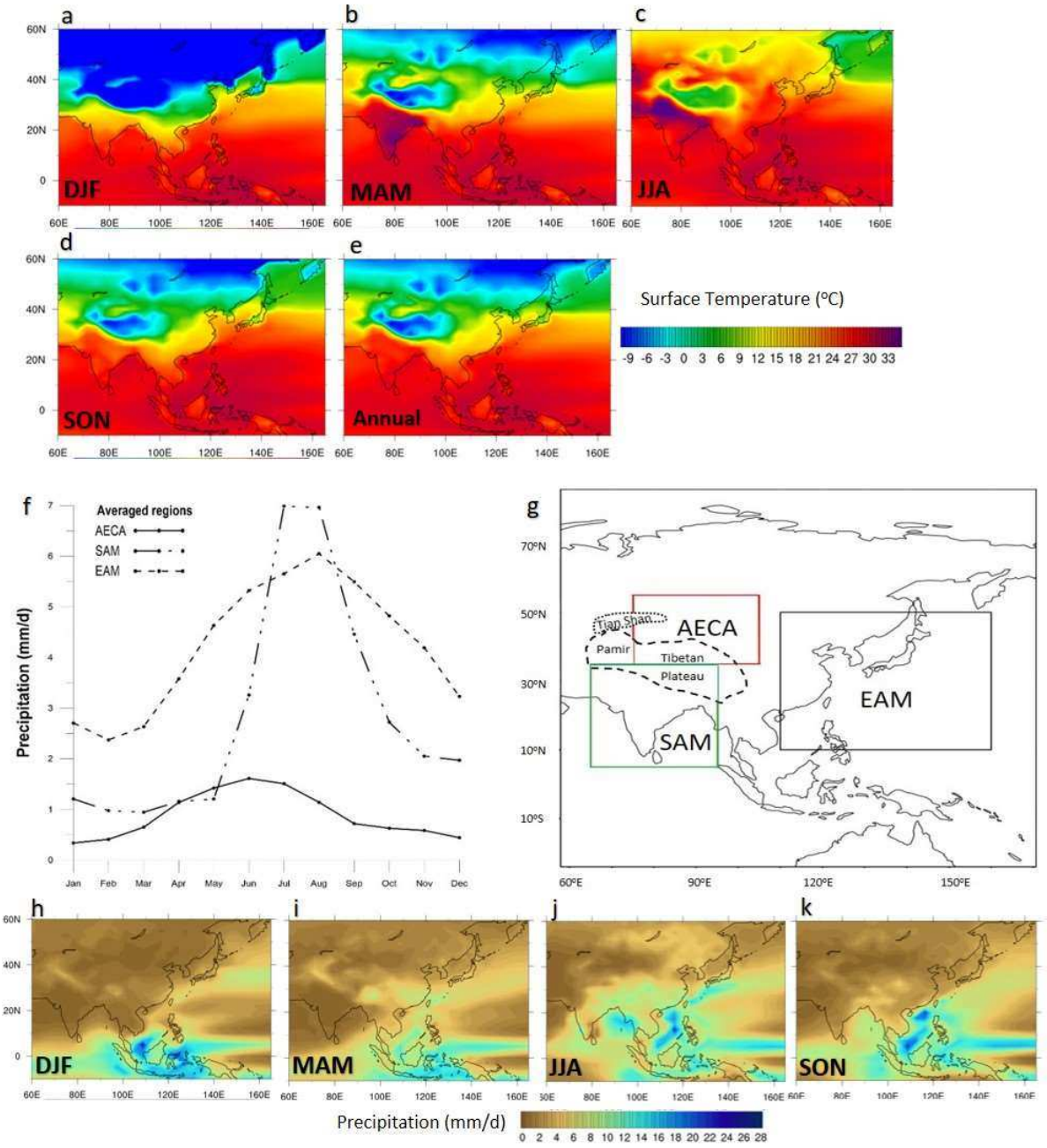

Fig. 2: a–e: Seasonal and annual surface temperature over the Asian continent and surrounding oceans. a) December – February (DJF), b) March – May (MAM), c) June – August (JJA) and d) September – November (SON), e) Annual mean surface temperature f) simulated PreInd annual precipitation cycle for the Arid East Central Asia (AECA, solid line), the South Asian Monsoon region (SAM, dash/dot line) and the East Asian Monsoon (EAM, dashed line), h-k: Seasonal simulated PreInd precipitation over the Asian continent and surrounding oceans, g) Regions selected to study each system's response to boundary condition changes. Green box: SAM, red box: AECA and black box: EAM regions. The map also shows the spatial extent of the TP, Tian Shan and Pamir orogens.

3. Results

3.1 Control simulation (annual precipitation and seasonal surface temperature)

The East Indian Monsoon region receives most of its rainfall from June to September (Parthasarathy et al., 1994). The annual precipitation (Fig. 2f-i) and temperature cycle (Fig. 2a-d) over the SAM region is successfully simulated in the preindustrial control experiment. Surface temperature and precipitation maximum values are reached during boreal summer (JJA) (Fig. 2h). During boreal winter (Fig. 2f), precipitation is focused around the equator and to the South. During spring (Fig. 2g), maximum precipitation migrates to the northeast towards the eastern part of China. In JJA precipitation is located in the tropical zone, around 20°N and as the summer gives way to autumn, precipitation is retreating away from the continental Asia and towards the Indian and Pacific Ocean (Fig.2i).

The EAM region is wetter throughout the year in comparison to the AECA and SAM regions (Fig. 2e). For all three regions the driest months are during boreal winter after which we observe an abrupt monsoon onset and a subsequent increase until peak rainfall is reached in late spring/early summer (for the AECA), and summer for SAM and EAM regions. (Fig.2e). The coldest period over Asia is during boreal winter with negative values reached in the temperate zone. However, the tropics and subtropics are constantly warm with temperatures higher than 25°C (Fig. 2a-d). The only season with surface temperatures over Asia always above 0°C is the boreal summer (Fig. 2c).

3.2 Impact of changing boundary conditions on the South Asian Monsoon

Analysis of the annual precipitation cycle over the SAM region for each of the experiments reveals a variety of responses to the different boundary condition changes (Fig. 3a-b) applied within the climate model. All simulations, except for the FlatTP, yield maximum precipitation values during July and August (Fig. 3a). After a doubling of atmospheric CO_2 July is no longer the month with the highest rainfall as values for August increase by 20% making August the month with the highest contribution to annual precipitation (Fig. 3b). However, this is not the highest increase observed in the 2piCO2

simulation as May precipitation over the SAM is 23% higher than in the PreInd. Quadrupling of CO_2 results in an increase from May until November with the highest increase simulated reaching 88% in May (Fig. 3b). Similarly to the 2piCO2 simulation, from January to April the model simulates a decrease of up to 37% (Fig. 3b). The only distinction between the double and quadruple CO_2 annual cycle patterns occurs in the monsoonal months. Specifically, during June and July the 2piCO2 precipitation is lower than the PreInd, whilst in 4piCO2 the same months are wetter by up to 35% (Fig. 3b). The removal of ice sheets plays a more important role over the SAM region under non-monsoonal circulation. Specifically, the months of Oct-Feb are wetter and during May (the month marking the monsoonal onset), the model simulates the largest change in precipitation indicating a more abrupt transition from non-monsoonal to monsoonal conditions (Fig. 3a-b).

Flattening of the TP changes the month with the highest precipitation values from July-August to May, but this is not the only notable change. Precipitation during January to April is minimal amongst all simulations (-70% the PreInd), accounting for the driest non-monsoonal months simulated (Fig. 3b). May and June receive more precipitation in the FlatTP simulation with higher values than the PreInd. However, the monsoonal months in the FlatTP simulation are generally drier with precipitation from July-September being the lower in comparison to all the other simulations (Fig. 3a). With the TP set to an Oligocene-like elevation, the most substantial change is predicted for May and June with precipitation increasing by more than 200% and 70% respectively (Fig.3b). With that increase in magnitude May is now contributing more than 10% in the annual rainfall indicating a steeper transition from non-monsoonal to monsoonal circulation (Fig.3a).

Simulated seasonal and annual temperature changes in response to altered boundary conditions do not show the same variations as precipitation (Fig. 4, S1, S2). The 2piCO2 and 4piCO2 simulations result in a higher annual surface temperature by up to 6^{o} and 12^{o}C respectively over the whole Asian continent and surrounding oceans (Fig. 4 a,b;). The SAM region becomes cooler by up to 1.5^{o}C in the NoGrIS simulation with the surface temperature over the Bay of Bengal and the Northern part of the Indian Ocean showing almost no change compared to the PreInd (change less than 0.5^{o}C) (Fig. 4c).

Removal of both the Greenland and Antarctic ice sheets leads to a cooling over the SAM region (Fig. 4d). The Indian landmass cools by up to 3°C. However, the southern flanks of the Himalayas experience higher temperatures of the same magnitude as the decrease compared to the PreInd (Fig. 4d). FlatTP simulated surface temperature is higher than the PreInd by 4°C over India, whilst the southern flanks of the Himalayas reach the highest simulated temperature with +13°C compared to the PreInd (Fig. 4e). For the SAM region the TP removal raises the surface temperature. The Bay of Bengal and the northernmost part of the Indian Ocean are simulated to have lower temperatures (up to -2°C compared to the PreInd) leading to a higher land – sea thermal contrast (Fig.4e). The Bay of Bengal and Indian Ocean in an Oligocene-like elevation setting show almost no change compared to the PreInd, while the Northern and Southern part of the Indian subcontinent cools by up to 9°C (Fig. 4f). Finally, in the Combo simulation the SAM region yields higher temperatures in both the Indian continent and the surrounding seas with a narrow strip of lower temperatures of about 5°C, parallel to the TP (Fig. 4g).

3.3 Impact of changing boundary conditions on the East Asian Monsoon

Doubling of atmospheric CO_2 produces wetter conditions from May to September by up to 18%, while non-monsoonal months experience small fluctuations that do not exceed 8% of the PreInd (Fig. 3c-d). Quadrupling of the CO_2 leads to higher monsoon related precipitation (May - September) with a notably high percentage increase (30%), while the non-monsoonal months (October to April) show changes that are less than 10% of the PreInd values (Fig. 3d). Under ice free conditions, the EAM region receives more precipitation during non-monsoonal months by up to 17% for February, while the monsoon related precipitation shows a slight decrease throughout the monsoonal period by up to 6.5% of the PreInd value (Fig. 3d). In the FlatTP simulation, precipitation is constantly lower than the PreInd with the exception of July and August where the model predicts a slight increase that does not exceed 2.5%, and thus can be considered negligible (Fig. 3d). Oligocene-like elevation for the TP results in the same pattern as in the FlatTP but with precipitation changes (relative to the PreInd) being less than in the FlatTP simulation. Specifically, non-monsoonal months show the highest decrease, by up

to 27%, whereas as in the FlatTP simulation the change during the monsoonal months can also be considered negligible with values of less than +3% (Fig. 3d). Where all changes have been made simultaneously (Combo) the resulting change in precipitation is more complex. Specifically, boreal winter and spring (December – May) experiences significantly lower precipitation (by up to -52%), even though precipitation for the monsoonal months (from July to September) shows higher values (the increase does not exceed 10% of the PreInd value) (Fig.3d).

For the EAM region, surface temperature under higher CO_2 values is almost 6°C greater over the Eastern Asian landmass, while the increase in the north-eastern Pacific is higher than PreInd by 2-3°C (Fig. 4a). In 4piCO2, the model simulates a constant increase in temperature with values reaching double the 2piCO2 values, and the Pacific Ocean cooler than the Eastern Asia landmass (Fig. 4b). Removing the Greenland ice sheet leads to lower temperatures for the whole EAM region with a temperature decrease of up to -3°C compared to the PreInd (Fig. 4c). NoIce conditions seem to mostly affect the northern and western part of the EAM region, while the Pacific Ocean experiences almost no change except for some small areas in proximity to the Eastern Asian landmass (Fig. 4d). The flattening of the TP generates elevated surface temperatures by up to 7°C in the mid and high latitudes of the EAM region, but the Pacific Ocean at 20°N shows with a cooling of up to 2.5°C (Fig. 4e). The OligTP simulation produces lower temperatures over the majority of the EAM region with values up to 2°C. However, the northern part of the EAM and parts of the Asian landmass are warmer by up to 2°C compared to the PreInd experiment (Fig. 4f). The EAM region for the Combo simulation yields higher temperatures by up to 6°C. The highest temperature changes are located in eastern China and around Japan while the surface temperature increases over the Pacific Ocean do not surpass 3°C (Fig.4g).

3.4 Impact of changing boundary conditions on the Arid East Central Asia

The response of the AECA to boundary condition changes is distinctly different to the regions analysed previously. In general, all of the simulations, except for the NoIce, produce wetter conditions over the

AECA with the largest change seen in the experiment FlatTP (Fig. 3e-f). Doubling atmospheric CO_2 increases the precipitation throughout the year, but the largest increase is simulated during non-monsoonal months (i.e. Jan, Feb) (Fig. 3e). Precipitation is also constantly higher in the 4piCO2 during all simulated months. From October to April Central Asia receives more precipitation (up to 100% more than the PreInd) (Fig. 3f). Removal of the Greenland ice-sheet leaves the AECA almost unaffected with precipitation difference from the PreInd never exceeding 10% (Fig. 3f). Completely removing the ice-sheets from both Greenland and Antarctica (NoIce) produces a decrease in precipitation throughout the year (Fig. 3e). Specifically, even though the months marking the monsoonal onset do not show large differences from the PreInd, from July to August the model simulates a constant decrease in precipitation that reaches its largest value during November (-31%) (Fig. 3f). The FlatTP simulation produces the largest increase in precipitation for the AECA region, with non-monsoonal months experiencing a large increase in rainfall with values more than two times the PreInd (Fig. 3f). Lower elevation of the TP (OligTP) also leads to increased precipitation throughout the year, but in contrast to the FlatTP simulation the increase is almost uniform throughout the whole year with an average of 42% (Fig. 3f). This uniform increase is not seen in the Combo simulation. Non monsoonal months receive more rainfall than the PreInd, which in some cases is greater than 100% the PreInd (Fig. 3f).

Surface temperature changes over the AECA region show the highest increase and decrease for any of the regions considered (Fig. 4). In 2piCO2, the AECA region becomes warmer by 6^{o}C on average, and this increases to 12^{o}C when CO_2 is quadrupled (Fig. 4a-b). Even though removing the Greenland ice-sheet generates a generally warmer climate, the AECA region shows only small fluctuations in temperature (Fig. 4c). The removal of both ice-sheets creates a complex pattern of surface temperature response with some areas experiencing higher than the PreInd temperatures and others lower (Fig. 4d). The magnitude of this change is ±5^{o}C. Flattening of the TP generates the highest change in the AECA region (Fig. 4e). Notably the region over the TP is warmer by up to 13^{o}C, while the rest of the AECA region shows an increase of up to 8^{o}C. The NW part of the AECA (North of the Tian Shan

274 orogen) is cooler than the PreInd by at least 3°C. Oligocene–like topography raises the surface
275 temperature over the TP just as in the FlatTP, with the main difference being the spatial extent of this
276 warming (Fig. 4f). In this case the region north of the TP is cooler by up to 5°C, but in the north-eastern
277 part of the AECA there is significant region with higher temperatures (Fig. 4f). Finally, the combination
278 of the boundary condition changes (Combo) generates much warmer conditions in the AECA
279 (compared to the PreInd) (Fig. 4g). Even though the TP is set to Oligocene elevation the spatial extent
280 of the high surface temperatures over the TP is similar to the FlatTP simulation, while to the north of
281 the AECA temperatures are also significantly higher (more than 8°C) (Fig. 4g).

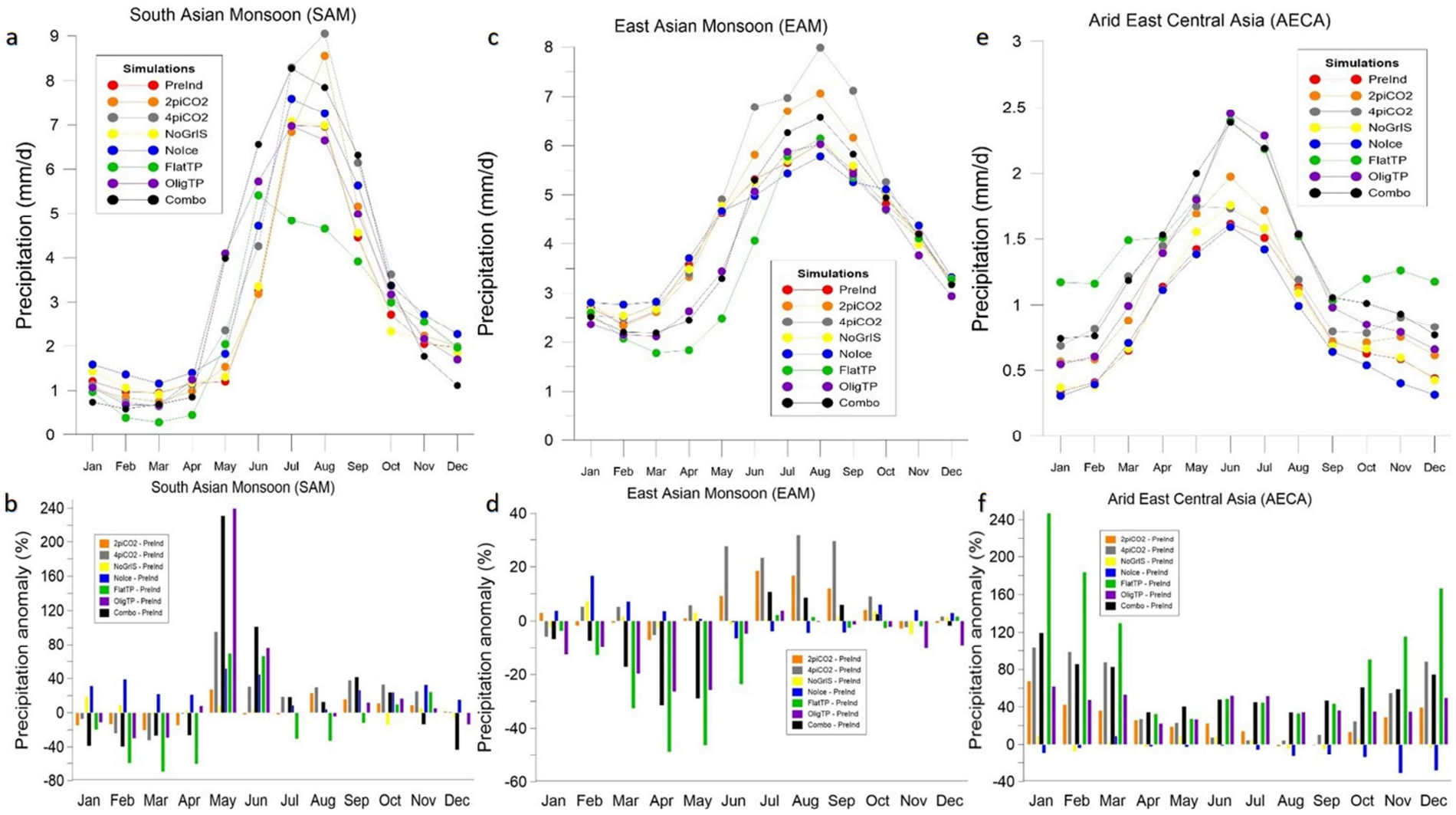
a
South Asian Monsoon (SAM)
Precipitation (mm/d)
Simulations
PreInd
2piCO2
4piCO2
NoGrIS
NoIce
FlatTP
OligTP
Combo
Jan Feb Mar Apr May Jun Jul Aug Sep Oct Nov Dec
b
South Asian Monsoon (SAM)
Precipitation anomaly (%)
2piCO2 - PreInd
4piCO2 - PreInd
NoGrIS - PreInd
NoIce - PreInd
FlatTP - PreInd
OligTP - PreInd
Combo - PreInd
c
East Asian Monsoon (EAM)
d
East Asian Monsoon (EAM)
e
Arid East Central Asia (AECA)
f
Arid East Central Asia (AECA)

282

283 **Fig. 3:** Averaged simulated monthly precipitation (mm/d) over: a) the SAM c) the EAM and e) the AECA regions and simulated percentage increase (positive values) and decrease (negative

284 values) in precipitation for each experiment compared to the pre-industrial control experiment for b) the SAM d) the EAM and f) the AECA regions.

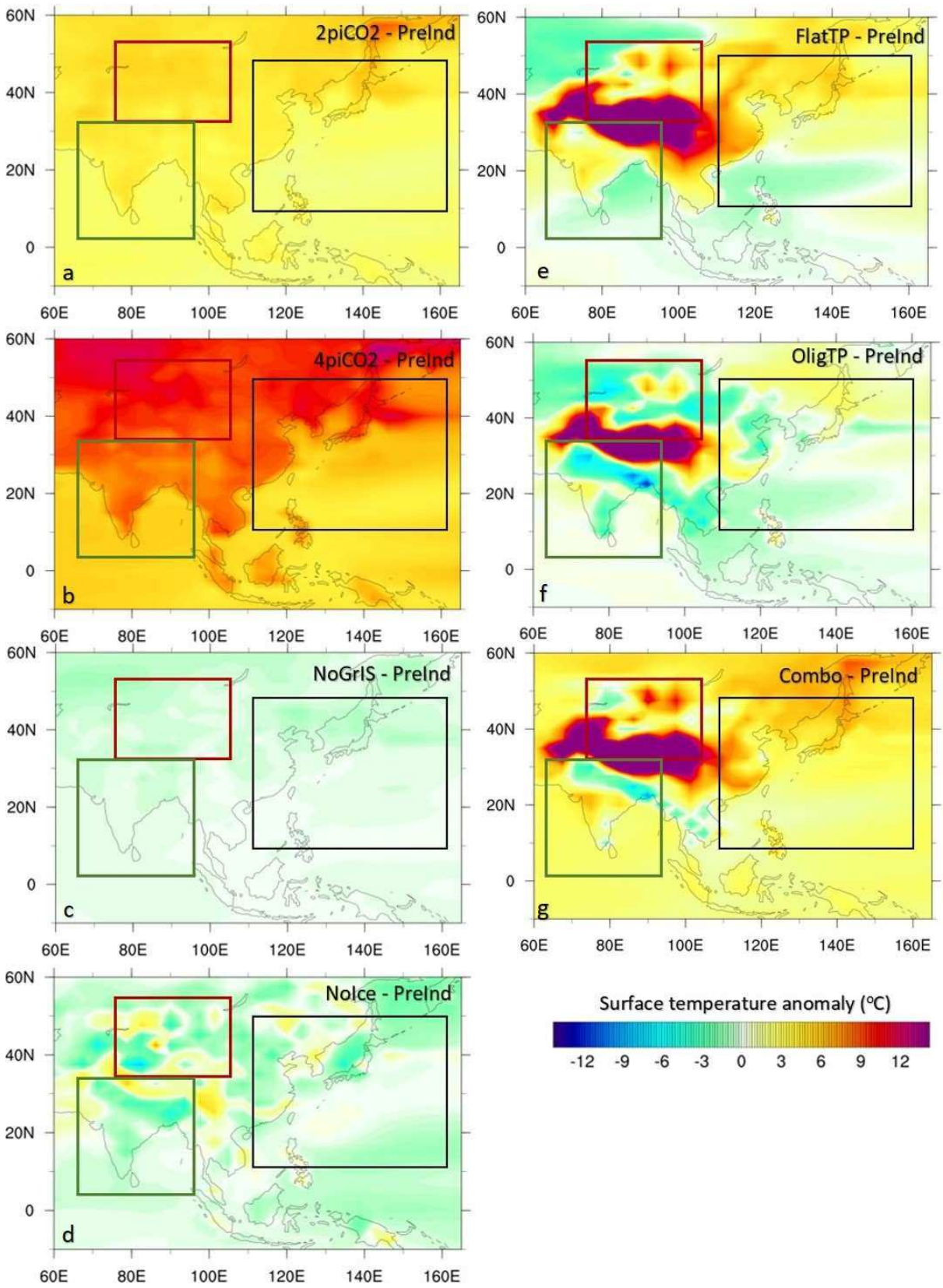

285

286 **Fig. 4:** Simulated annual surface temperature anomaly (°C) compared to the PreInd for: a) 2piCO2, b) 4piCO2, c) NoGrIS, d)

287 NoIce, e) FlatTP, f) OligTP and g) Combo simulation. The SAM, EAM and AECA regions are denoted by the green, black and

288 red boxes respectively.

4. Discussion

4.1 Boundary condition effects on climate and the monsoons

Increased atmospheric CO_2 leads to enhanced heating of the Earth (Fig. 4a-b) (IPCC, 2001) and its radiative forcing alters the atmospheric heat distribution and hydrological cycle (Cherchi et al., 2011). The land-sea thermal contrast is the basic forcing mechanism for the SAM, and an increased contrast can be expected to strengthen monsoon circulation (Turner et al., 2011).

The modelled monsoonal precipitation under elevated CO_2 concentrations increases over the SAM and EAM regions, consistent with previous modelling studies (i.e. Annamalai et al., 2007), and is a product of enhanced moisture transport from a warmer Indian Ocean towards the Asian continent (Ueda et al., 2006). Our results indicate increased monsoonal precipitation for both the 2piCO2 and 4piCO2 simulations for the SAM and EAM regions following the "wet-get-wetter response" (Held and Soden, 2006; Fig. 5b-c). This suggests that precipitation in regions that already have strong moisture convergence and precipitation will be enhanced (Chou et al., 2009). During the monsoonal months, the moisture availability over the SAM and EAM shows an increase consistent with higher precipitation (Fig. 7b-c), while the high pressure systems over the AECA and East EAM regions retreat to the West and East respectively (Fig. 9b-c). In the PreInd simulation the low pressure system associated with precipitation is located above the TP, while, in 2piCO2, the low pressure system expands to the North and East of the TP (Fig. 9b). Additionally, the precipitation simulated over the SAM region in 4piCO2, where surface temperature reaches higher values throughout the year (Fig. 4b), shows a precipitation enhancement following the traditional monsoon period suggesting a possible extension in the duration of the monsoon (Fig. 3a). At the same time the beginning of the monsoonal period (May) receives more precipitation leading to a steeper transition from non-monsoonal to monsoonal conditions (Fig. 3a, 6). The AECA in both the 2piCO2 and 4piCO2 simulations does not receive more precipitation under monsoonal circulation, while Precipitation – Evaporation (P – E) shows a localized decrease without significant change in the pattern from the PreInd (Fig. 7b-c). Under non-monsoonal

circulation, moisture availability over the SAM and EAM regions shifts from positive (during the monsoons) to negative, even over the landmass of the EAM region where precipitation shows an increase (Fig. 8b-c). However, the adjacent Indian Ocean now shows increased moisture availability. Interestingly, during non-monsoonal months the AECA receives more precipitation by at least 0.5 mm/d (for 2piCO2) up to 1 mm/d (for 4piCO2), which in an arid area corresponds to an increase of 34% and 71% respectively (Fig. 6b-c). Correspondingly, from Oct – Apr, P – E over the AECA indicates enhanced moisture availability and therefore less arid conditions with increasing CO_2 values (Fig. 8b-c). During the non-monsoon months the high pressure system over Central Asia shrinks and migrates northwards producing lower pressure over the AECA region compared to the PreInd (Fig. 10b-c).

The removal of the Greenland ice-sheet creates only localised changes and does not seem to affect Asian climate in a significant way (Fig. 5d). In NoIce the simulated surface temperature is lower than in the PreInd for most of the SAM, EAM and AECA regions (Fig. 4d). However, monsoonal precipitation exceeds the PreInd demonstrating that the land-sea thermal contrast is not the only driver of monsoon intensification. This can be explained if we see the monsoon as a manifestation of the ITCZ seasonal migration in response to the positioning of the maximum insolation (Gadgil, 2003). Our simulation reveals that the removal of the Antarctic ice-sheet yields a warmer equatorial Indian Ocean during boreal summer, leading to a migration of the ITCZ to the North towards inland India. Furthermore, reinforced southerlies and westerlies carry moisture from the North part of the Indian Ocean and Bay of Bengal towards inland south Asia increasing the moisture availability, not only over the SAM region but also over the landmass of the EAM and the area located in between those systems (Fig. 7e, 9e).

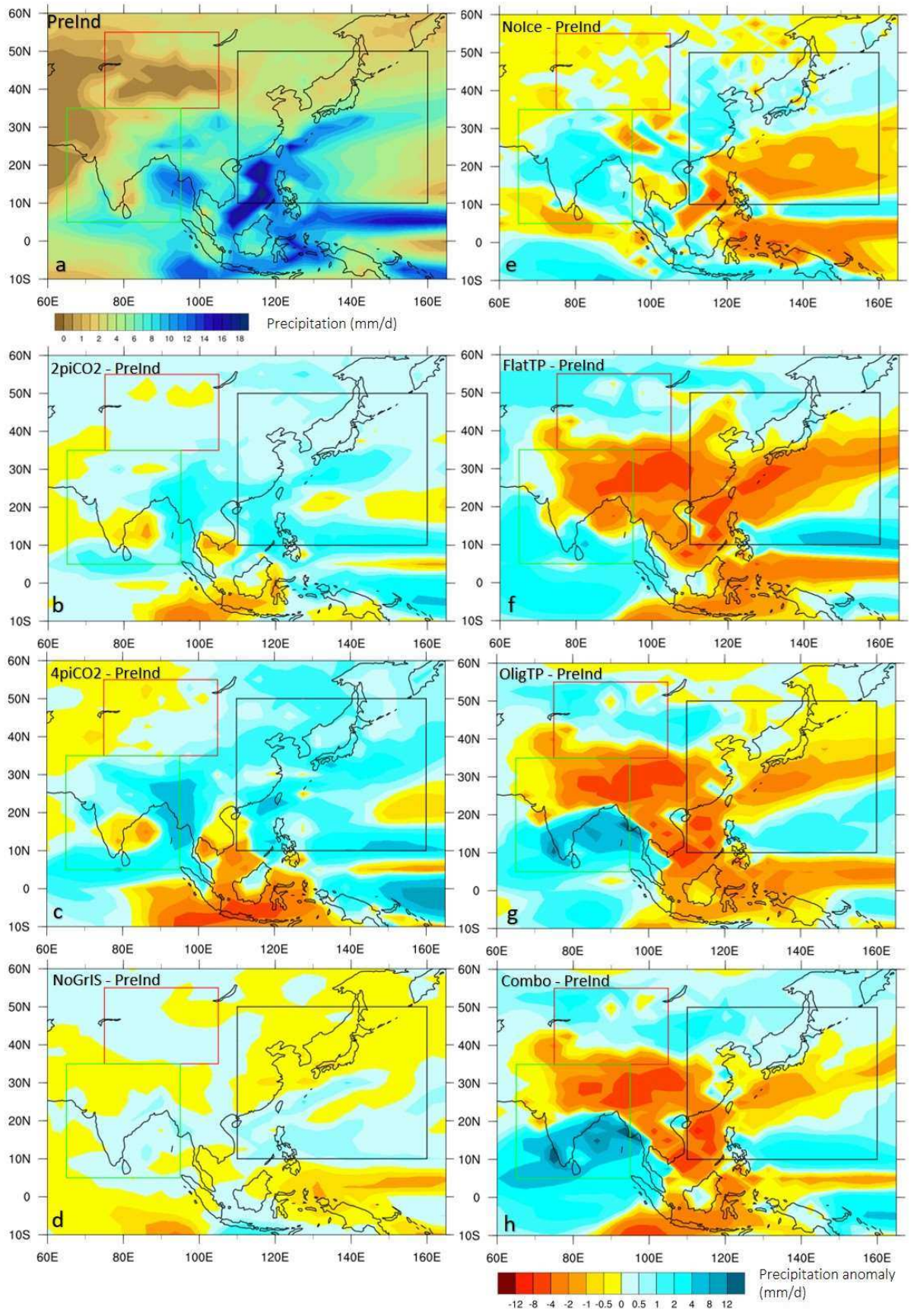

334

335 **Fig. 5:** a) Simulated monsoonal (May – September) precipitation (mm/d) for the PreInd. Simulated monsoonal precipitation

336 anomaly (mm/d) compared to the PreInd for: b) 2piCO2, c) 4piCO2, d) NoGrIS, e) NoIce, f) FlatTP, g) OligTP and h) Combo

337 simulations. The SAM, EAM and AECA regions are denoted by the green, black and red boxes respectively.

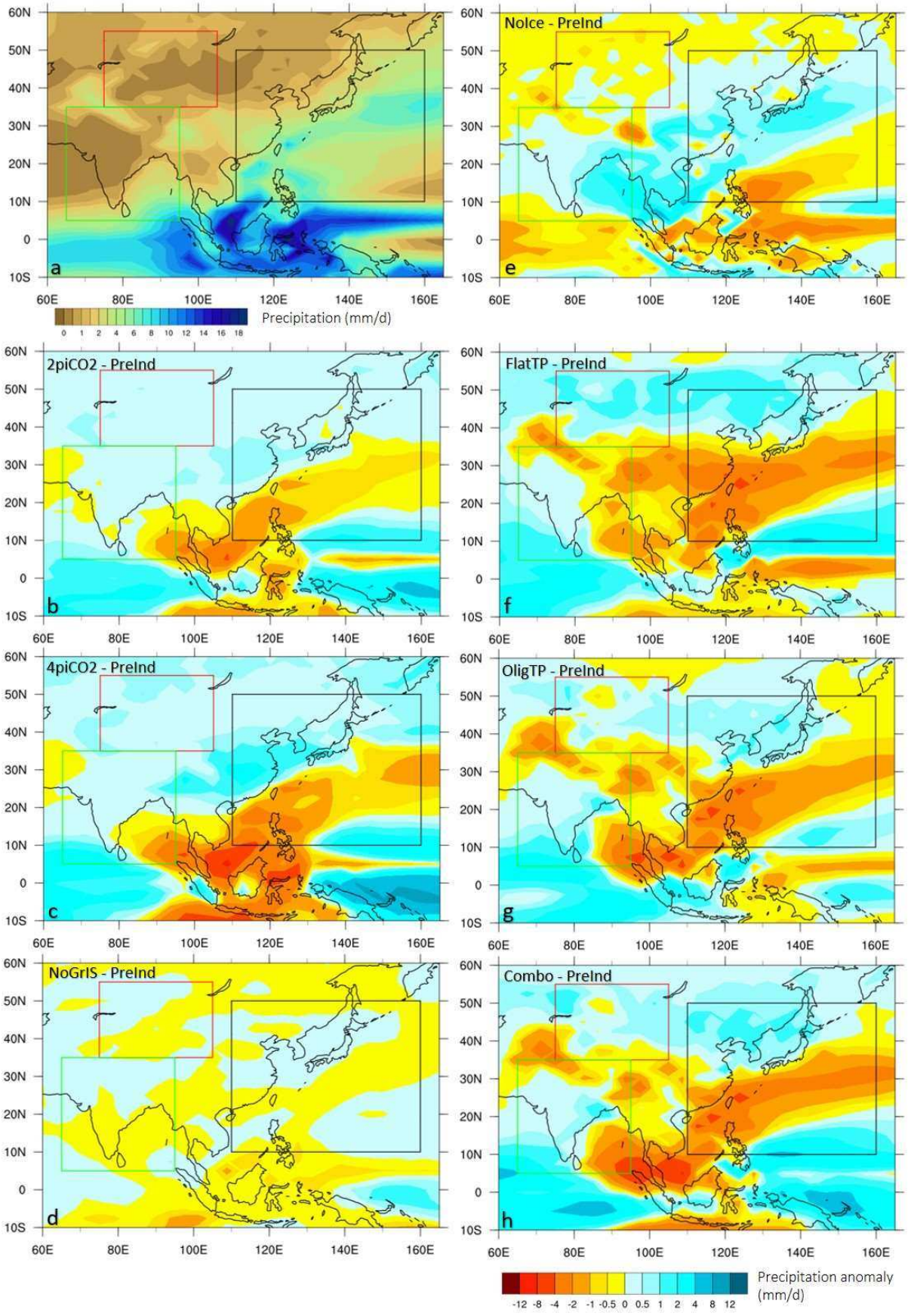

338

Fig. 6: a) Simulated non-monsoonal (October – April) precipitation (mm/d) for the PreInd. Simulated non-monsoonal precipitation anomaly (mm/d) compared to the PreInd for: b) 2piCO2, c) 4piCO2, d) NoGrIS, e) NoIce, f) FlatTP, g) OligTP and h) Combo simulations. The SAM, EAM and AECA regions are denoted by the green, black and red boxes respectively.

During the monsoonal months, moisture availability and mean sea level pressure does not show a large difference from the PreInd (Fig. 7e, 9e) for all the three regions.

With the TP flattened temperatures over the land are constantly higher throughout the year (Fig. 4e), however, in opposition to the 2piCO2 and 4piCO2, where the temperature change is almost uniform above the Asian landmass and precipitation was intensified, in FlatTP the Asian monsoon related precipitation becomes weaker (Fig. 3a-d). Precipitation rates are the lowest amongst all simulations performed, and for the first time we observe a shift of this magnitude in the moisture availability over Asia (Fig. 7,8 f). This can be attributed to the up to 13^{o}C higher than PreInd temperatures over the whole Asian landmass (Fig. 4e). Notably, during monsoonal months, the AECA reaches the lowest values of P – E with a change not only in the magnitude but more importantly in its spatial distribution (Fig. 7f). The position of the negative moisture availability zone falls between the two low pressure systems that are created over Asia when the TP is removed (Fig. 9f). With no orographic barrier in place, atmospheric pressure systems over Asia from Oct – Apr is centred at 50^{o}N while in the FlatTP simulation, is centred at 35^{o}N, with less spatial extent and lower values (Fig. 10f). Nevertheless, during non-monsoonal months the AECA shows positive moisture availability and as a result precipitation reaches the highest percentage of increase compared to the PreInd (on average 144% increase from Oct-Apr) (Fig.8f). This increase can be attributed to the change in moisture availability as westerlies are enhanced over the AECA since the high pressure system is displaced to the South and the area of the pressure change is within the AECA region (Fig. 10f).

In the OligTP simulation, the EAM region receives less precipitation than in PreInd indicating a weaker monsoon where moisture availability from the adjacent water bodies is decreasing (Fig. 7g, 3c-d). With the TP set to Oligocene elevation the SAM precipitation intensifies especially in the beginning of the monsoon (May-June) (Fig. 3a). Wetter conditions are also simulated for the AECA that combined with

365 the different moisture availability and low pressure patterns (compared to the FlatTP), indicates that
366 there is a threshold to the TP elevation that is controlling the aridity and monsoon intensity (Fig. 7g,
367 9g) that was probably established after the Oligocene. Even under non-monsoonal circulation the
368 AECA is constantly wetter by up to 60% (Fig. 3f) also suggesting that the aridity over the region was
369 established after the Oligocene.

370 Finally, in the Combo simulation we observe that the simulated climate over Asia is mainly driven by
371 the topography change rather than the CO_2 increase or the ice-sheet formation (Fig. 7h, 8h).

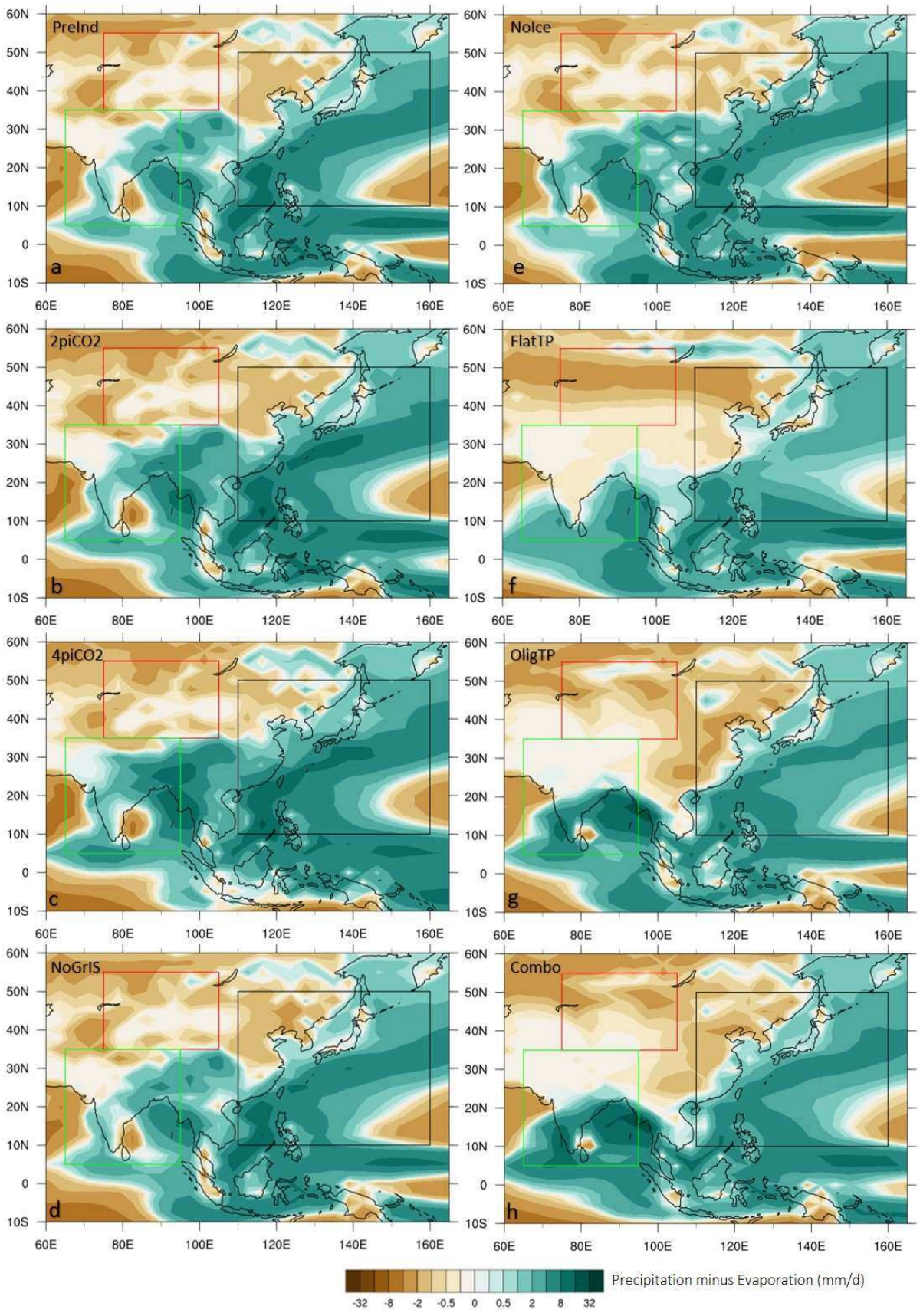

372

373 **Fig. 7:** Simulated monsoonal (May – September) Precipitation – Evaporation (P – E) for: a) PreInd b) 2piCO2, c) 4piCO2, d)

NoGrIS, e) NoIce, f) FlatTP, g) OligTP and h) Combo simulations. The SAM, EAM and AECA regions are denoted by the green, black and red boxes respectively.

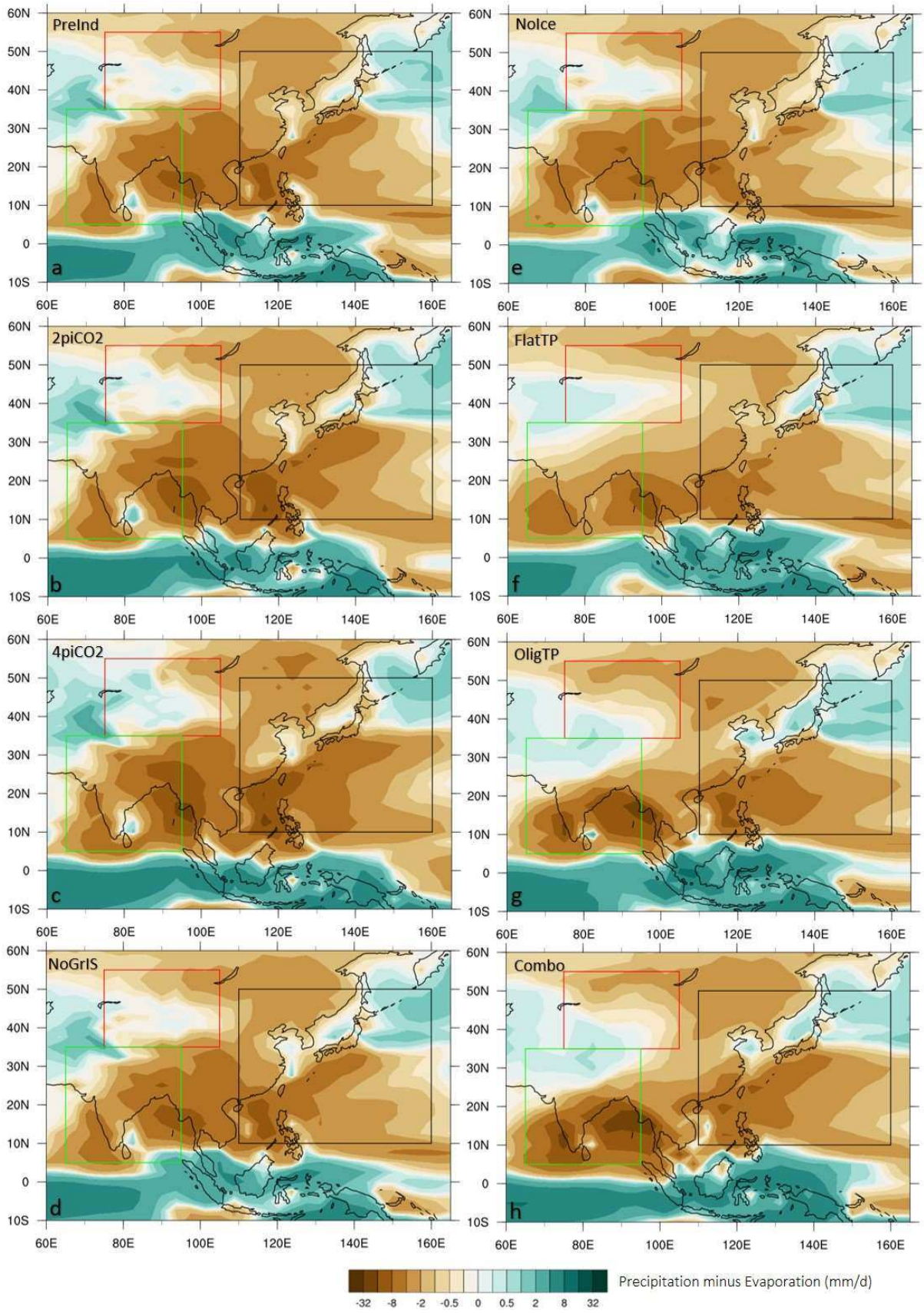

Fig. 8: Simulated non - monsoonal (October – April) Precipitation – Evaporation (P – E) for: a) PreInd b) 2piCO2, c) 4piCO2, d) NoGrIS, e) NoIce, f) FlatTP, g) OligTP and h) Combo simulations. The SAM, EAM and AECA regions are denoted by the green, black and red boxes respectively.

4.2 Significance of results for understanding the development of aridity in Asia during the Cenozoic

Changes in atmospheric CO_2 concentration, Antarctic ice-sheet coverage and TP elevation have all been determined to be important drivers for the precipitation that the SAM and EAM regions receive, not only during monsoonal months but during non-monsoonal months (Fig. 5, 6). Nevertheless, the AECA region seems to remain unaffected by all changes to boundary conditions except for the TP elevation for both monsoonal and non-monsoonal months. In a palaeoclimate context it has been well established that the differential uplift of the TP, together with associated land/sea distribution changes as well as the global cooling at the EOT, played a significant role in the climatic evolution of the Asian continent in general. However, aridification of inland Asia is interpreted as a combination of the global oceanic cooling and ice-sheet growth, the TP uplift and the retreat of the Paratethys Sea (Bosboom et al., 2014a, b; Licht et al., 2014; Lippert et al., 2014). Our sensitivity experiments indicate that the Asian aridification is solely controlled by the TP uplift rather than changes in CO_2 and ice-sheet formation. From the precipitation and P – E results analysed in this study, it is clear that climate reconstructions from proxy records can be challenging to interpret for a number of reasons. Firstly, the nature of climate variability recorded by different proxies varies. Some proxy systems (either physical/chemical or biological) may record annual environmental conditions averaged over long timescales. Others may provide information useful to deduce seasonality and the relative strength of the monsoons. So, understanding the nature of what proxy system is actually recording in the environment will be central in any comparison to the climate model results shown here. Secondly, given the spatially heterogeneity seen in our model results, the geographical location of any proxy data record will be an important predetermining factor in the environmental reconstruction itself. For example, during the monsoonal period in the 4piCO2 experiment, the AECA region receives more precipitation on average. However, the western part of the same region is drier compared to the

PreInd (Fig. 5c). Thus, extrapolation from a single proxy record from the west part of the AECA could lead to a completely different environmental reconstruction than a proxy collected from the eastern part of the same region. Finally, depending on what each proxy records (i.e. precipitation or P – E), the most important driver can be different. Specifically, if one focusses on P – E in the EAM region for the OligTP simulation during non-monsoonal months (Fig. 8g), we would expect to have greater moisture availability in the environment. However, the results for precipitation alone (which declines relative to the PreInd), would suggest otherwise (Fig. 6g).

Finally, in order to understand and decipher the forcings and underlying mechanisms that drove the aridity and monsoonal circulation after the EOT in more detail, it is necessary to perform an additional series of fully realistic Oligocene simulations, whereby the effect of individual boundary condition changes can be fully factorized.

Conclusions

Using HadCM3, we attempt to determine the effect of three different factors to Asian climate (CO_2, ice-sheet coverage and Tibetan Plateau uplift). Our model shows that CO_2 increase leads to enhanced monsoonal precipitation for both the South Asian Monsoon and East Asian Monsoon and wetter conditions over Arid East Central Asia throughout the year. The Greenland ice-sheet seems to not affect Asian climate. However, the specification of Antarctic ice-sheet produces a wetter Arid East Central Area, stronger South Asian Monsoon conditions but weaker East Asian Monsoon related precipitation. Tibetan Plateau uplift corresponds to an intensified South Asian Monsoon but weakens the East Asian Monsoon region's precipitation through the year. A combination of boundary condition changes seems to follow the OligTP simulation's general pattern with wetter conditions over the Arid East Central Asia, throughout the year, a steeper transition from non-monsoonal to monsoonal precipitation for the South, and a weaker precipitation over East Asia during the boreal winter. This suggests that the TP, even though other changes contribute, is the main driver for climatic change over Asia. Finally, by studying different hydroclimatic parameters (i.e. Precipitation vs Precipitation –

Evaporation) we show that the relative significance of each forcing is dependent on the parameter studied itself, a fact that should be taken into consideration when interpreting proxy records for palaeoclimate reconstructions.

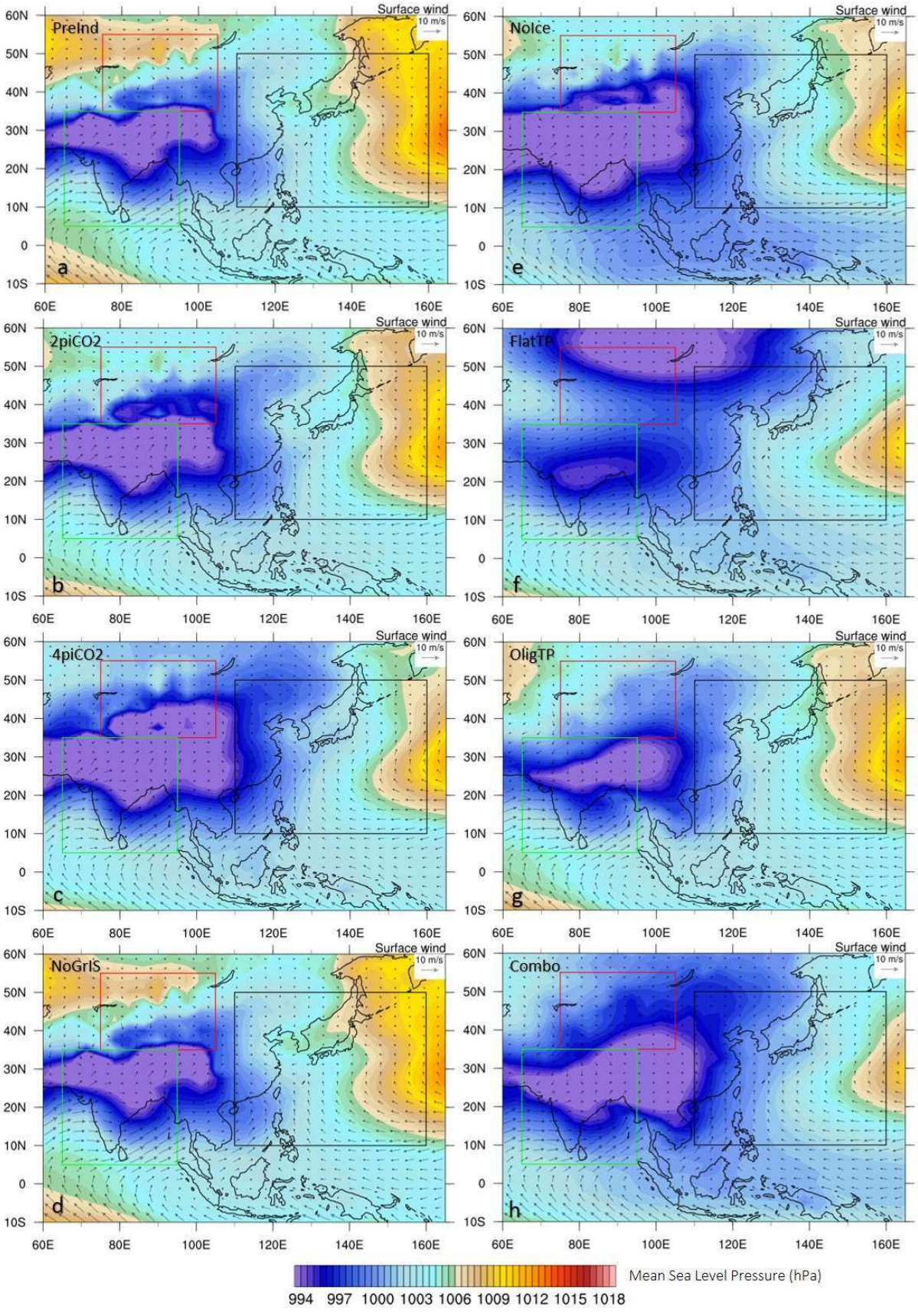
PreInd
Surface wind
10 m/s
a
NoIce
e
2piCO2
b
FlatTP
f
4piCO2
c
OligTP
g
NoGrIS
d
Combo
h
60N
50N
40N
30N
20N
10N
0
10S
60E
80E
100E
120E
140E
160E
Mean Sea Level Pressure (hPa)
994 997 1000 1003 1006 1009 1012 1015 1018

431

Fig. 9: Simulated monsoonal (May - September) Mean Sea Level Pressure and surface winds for: a) PreInd b) 2piCO2, c) 4piCO2, d) NoGrIS, e) NoIce, f) FlatTP, g) OligTP and h) Combo simulations. The SAM, EAM and AECA regions are denoted by the green, black and red boxes respectively.

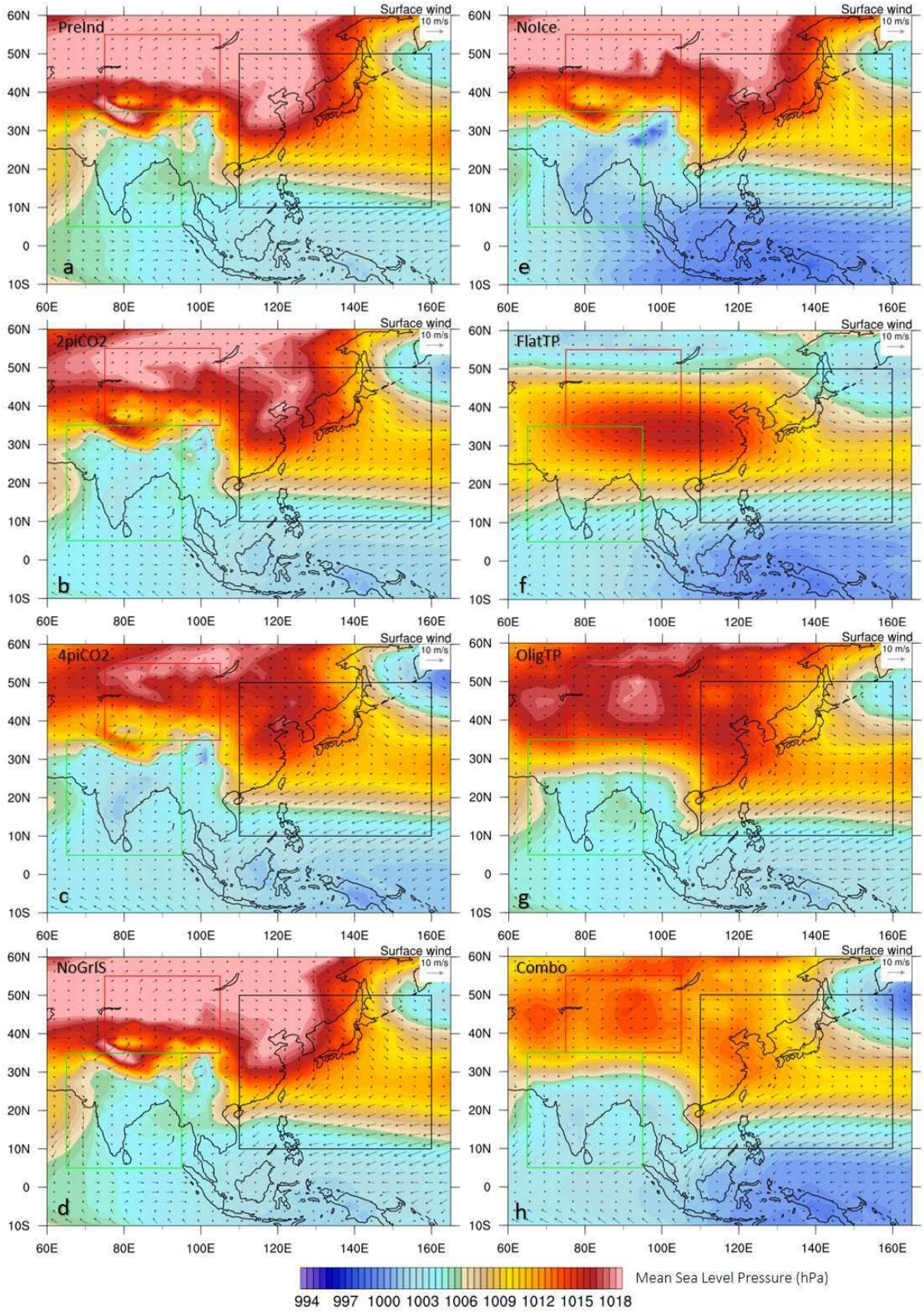
PreInd
NoIce
2piCO2
FlatTP
4piCO2
OligTP
NoGrIS
Combo
a
b
c
d
e
f
g
h
Surface wind
10 m/s
60N
50N
40N
30N
20N
10N
0
10S
60E
80E
100E
120E
140E
160E
Mean Sea Level Pressure (hPa)
994 997 1000 1003 1006 1009 1012 1015 1018

435

Fig. 10: Simulated non-monsoonal (October - April) Mean Sea Level Pressure and surface winds for: a) PreInd b) 2piCO2, c) 4piCO2, d) NoGrIS, e) NoIce, f) FlatTP, g) OligTP and h) Combo simulations. The SAM, EAM and AECA regions are denoted by the green, black and red boxes respectively.

References

An, Z., Kutzbach, J.E., Prell, W.L., Porter, S.C., 2001. Evolution of Asian monsoons and phased uplift of the Himalaya-Tibetan plateau since Late Miocene times. Nature 411, 62–66. https://doi.org/10.1038/35075035

Annamalai, H., Hamilton, K., Sperber, K.R., 2007. The South Asian Summer Monsoon and Its Relationship with ENSO in the IPCC AR4 Simulations. J. Clim. 20, 1071–1092. https://doi.org/10.1175/JCLI4035.1

Ao, H., Roberts, A.P., Dekkers, M.J., Liu, X., Rohling, E.J., Shi, Z., An, Z., Zhao, X., 2016. Late Miocene–Pliocene Asian monsoon intensification linked to Antarctic ice-sheet growth. Earth Planet. Sci. Lett. 444, 75–87. https://doi.org/10.1016/j.epsl.2016.03.028

Bosboom, R., Dupont-Nivet, G., Grothe, A., Brinkhuis, H., Villa, G., Mandic, O., Stoica, M., Huang, W., Yang, W., Guo, Z., Krijgsman, W., 2014. Linking Tarim Basin sea retreat (west China) and Asian aridification in the late Eocene. Basin Res. 26, 621–640. https://doi.org/10.1111/bre.12054

Bosboom, R.E., Abels, H.A., Hoorn, C., van den Berg, B.C.J., Guo, Z., Dupont-Nivet, G., 2014. Aridification in continental Asia after the Middle Eocene Climatic Optimum (MECO). Earth Planet. Sci. Lett. 389, 34–42. https://doi.org/10.1016/j.epsl.2013.12.014

Cherchi, A., Alessandri, A., Masina, S., Navarra, A., 2011. Effects of increased CO2 levels on monsoons. Clim. Dyn. 37, 83–101. https://doi.org/10.1007/s00382-010-0801-7

Chou, C., Neelin, J.D., Chen, C.A., Tu, J.Y., 2009. Evaluating the “rich-get-richer” mechanism in tropical precipitation change under global warming. J. Clim. 22, 1982–2005. https://doi.org/10.1175/2008JCLI2471.1

Cox, P.M., Betts, R.A., Bunton, C.B., Essery, R.L.H., Rowntree, P.R., Smith, J., 1999. The impact of new

land surface physics on the GCM simulation of climate and climate sensitivity. Clim. Dyn. 15, 183–203. https://doi.org/10.1007/s003820050276

Dabang, J., Huijun, W., Xianmei, L., 2005. Evaluation of East Asian climatology as simulated by seven coupled models. Adv. Atmos. Sci. 22, 479–495. https://doi.org/10.1007/BF02918482

DeCelles, P.G., Quade, J., Kapp, P., Fan, M., Dettman, D.L., Ding, L., 2007. High and dry in central Tibet during the Late Oligocene. Earth Planet. Sci. Lett. 253, 389–401. https://doi.org/10.1016/j.epsl.2006.11.001

DeConto, R.M., Pollard, D., Wilson, P.A., Pälike, H., Lear, C.H., Pagani, M., 2008. Thresholds for Cenozoic bipolar glaciation. Nature 455, 652–656. https://doi.org/10.1038/nature07337

Dupont-Nivet, G., Hoom, C., Konert, M., 2008. Tibetan uplift prior to the Eocene-Oligocene climate transition: Evidence from pollen analysis of the Xining Basin. Geology 36, 987–990. https://doi.org/10.1130/G25063A.1

Dupont-Nivet, G., Krijgsman, W., Langereis, C.G., Abels, H.A., Dai, S., Fang, X., 2007. Tibetan plateau aridification linked to global cooling at the Eocene–Oligocene transition. Nature 445, 635–638. https://doi.org/10.1038/nature05516

Gadgil, S., 2003. The Indian Monsoon and its variability. Annu. Rev. Earth Planet. Sci. 65, 349–369. https://doi.org/10.1146/annurev.physiol.65.092101.142156

Gordon, C., Cooper, C., Senior, C.A., Banks, H., Gregory, J.M., Johns, T.C., Mitchell, J.F.B., Wood, R.A., 2000. The simulation of SST, sea ice extents and ocean heat transports in a version of the Hadley Centre coupled model without flux adjustments. Clim. Dyn. 16, 147–168. https://doi.org/10.1007/s003820050010

Guo, Z.T., Ruddiman, W.F., Hao, Q.Z., Wu, H.B., Qiao, Y.S., Zhu, R.X., Peng, S.Z., Wei, J.J., Yuan, B.Y., Liu, T.S., 2002. Onset of Asian desertification by 22 Myr ago inferred from loess deposits in China. Nature 416, 159–163. https://doi.org/10.1038/416159a

485 Held, I.M., Soden, B.J., 2006. Robust responses of the hydrologic cycle to global warming. J. Clim. 19,
486 5686–5699. https://doi.org/10.1175/JCLI3990.1
487 Hong, B., Gasse, F., Uchida, M., Hong, Y., Leng, X., Shibata, Y., An, N., Zhu, Y., Wang, Y., 2014.
488 Increasing summer rainfall in arid eastern-Central Asia over the past 8500 years. Sci. Rep. 4, 1–
489 10. https://doi.org/10.1038/srep05279
490 Hunter, S.J., Haywood, A.M., Valdes, P.J., Francis, J.E., Pound, M.J., 2013. Modelling equable climates
491 of the Late Cretaceous: Can new boundary conditions resolve data–model discrepancies?
492 Palaeogeogr. Palaeoclimatol. Palaeoecol. 392, 41–51.
493 https://doi.org/10.1016/j.palaeo.2013.08.009
494 Inness, P.M., Slingo, J.M., 2003. Simulation of the Madden-Julian oscillation in a coupled general
495 circulation model. Part I: Comparison with observations and an atmosphere-only GCM. J. Clim.
496 16, 345–364. https://doi.org/10.1175/1520-0442(2003)016<0345:SOTMJO>2.0.CO;2
497 Ipcc, 2001. Model Evaluation. Work. Gr. I Sci. basis 54.
498 Jian, X., Guan, P., Fu, S.-T., Zhang, D.-W., Zhang, W., Zhang, Y.-S., 2014. Miocene sedimentary
499 environment and climate change in the northwestern Qaidam basin, northeastern Tibetan
500 Plateau: Facies, biomarker and stable isotopic evidences. Palaeogeogr. Palaeoclimatol.
501 Palaeoecol. 414, 320–331. https://doi.org/10.1016/j.palaeo.2014.09.011
502 Khon, V.C., Wang, Y. V., Krebs-Kanzow, U., Kaplan, J.O., Schneider, R.R., Schneider, B., 2014. Climate
503 and CO2 effects on the vegetation of southern tropical Africa over the last 37,000 years. Earth
504 Planet. Sci. Lett. 403, 407–417. https://doi.org/10.1016/j.epsl.2014.06.043
505 Kutzbach, J.E., Liu, Z., 1997. Response of the African Monsoon to Orbital Forcing and Ocean
506 Feedbacks in the Middle Holocene. Science (80-.). 278, 440 LP-443.
507 Lefebvre, V., Donnadieu, Y., Goddéris, Y., Fluteau, F., Hubert-Théou, L., 2013. Was the Antarctic
508 glaciation delayed by a high degassing rate during the early Cenozoic? Earth Planet. Sci. Lett.
509 371–372, 203–211. https://doi.org/10.1016/j.epsl.2013.03.049

Licht, A., van Cappelle, M., Abels, H.A., Ladant, J.-B., Trabucho-Alexandre, J., France-Lanord, C., Donnadieu, Y., Vandenberghe, J., Rigaudier, T., Lécuyer, C., Terry Jr, D., Adriaens, R., Boura, A., Guo, Z., Soe, A.N., Quade, J., Dupont-Nivet, G., Jaeger, J.-J., 2014. Asian monsoons in a late Eocene greenhouse world. Nature 513, 501–506. https://doi.org/10.1038/nature13704

Lippert, P.C., van Hinsbergen, D.J.J., Dupont-Nivet, G., 2014. Early Cretaceous to present latitude of the central proto-Tibetan Plateau: A paleomagnetic synthesis with implications for Cenozoic tectonics, paleogeography, and climate of Asia. Geol. Soc. Am. Spec. Pap. 2507, 1–21. https://doi.org/10.1130/2014.2507(01)

Liu, X.D., Dong, B.W., 2013. Influence of the Tibetan Plateau uplift on the Asian monsoon-arid environment evolution. Chinese Sci. Bull. 58, 4277–4291. https://doi.org/10.1007/s11434-013-5987-8

Lunt, D.J., Flecker, R., Clift, P.D., 2010. The impacts of Tibetan uplift on palaeoclimate proxies. Geol. Soc. London, Spec. Publ. 342, 279–291. https://doi.org/10.1144/SP342.16

Markwick, P.J., 2007. The palaeogeographic and palaeoclimatic significance of climate proxies for data-model comparisons. Deep. Perspect. Clim. Chang. Marrying Signal from Comput. Model. Biol. Proxies 251–312.

Molnar, Peter, England, Philip, Martinod, J., 1993. Mantle dynamics, uplift of the Tibetan Plateau and the Indian monsoon.

Molnar, P., Boos, W.R., Battisti, D.S., 2010. Orographic Controls on Climate and Paleoclimate of Asia: Thermal and Mechanical Roles for the Tibetan Plateau. Annu. Rev. Earth Planet. Sci. 38, 77–102. https://doi.org/10.1146/annurev-earth-040809-152456

Pagani, M., Zachos, J.C., Freeman, K.H., Tipple, B., Bohaty, S., 2005. Marked Decline in Atmospheric Carbon Dioxide Concentrations During the Paleogene. Science (80-.). 309, 600 LP-603. https://doi.org/10.1126/science.1110063

Parthasarathy, B., Munot, A.A., Kothawale, D.R., 1994. All-India monthly and seasonal rainfall series:

1871-1993. Theor. Appl. Climatol. 49, 217–224. https://doi.org/10.1007/BF00867461

Pearson, P.N., Foster, G.L., Wade, B.S., 2009. Atmospheric carbon dioxide through the Eocene-Oligocene climate transition. Nature 461, 1110–1113. https://doi.org/10.1038/nature08447

Qian, Y., Flanner, M.G., Leung, L.R., Wang, W., 2011. Sensitivity studies on the impacts of Tibetan Plateau snowpack pollution on the Asian hydrological cycle and monsoon climate. Atmos. Chem. Phys. 11, 1929–1948. https://doi.org/10.5194/acp-11-1929-2011

Rowley, D.B., Currie, B.S., 2006. Palaeo-altimetry of the late Eocene to Miocene Lunpola basin, central Tibet. Nature 439, 677–681. https://doi.org/10.1038/nature04506

Smith, R.N.B., 1990. A scheme for predicting layer clouds and their water content in a general circulation model. Q. J. R. Meteorol. Soc. 116, 435–460. https://doi.org/10.1002/qj.49711649210

Turner, A., Sperber, K.R., Slingo, J., Meehl, G., Mechoso, C.R., Kimoto, M., Giannini, A., 2011. Modelling Monsoons: Understanding and Predicting Current and Future Behaviour. Glob. Monsoon Syst. Res. Forecast 2nd Editio, 421–454.

Turner, a. G., Inness, P.M., Slingo, J.M., 2005. The role of the basic state in the ENSO–monsoon relationship and implications for predictability. Q. J. R. Meteorol. Soc. 131, 781–804. https://doi.org/10.1256/qj.04.70

Ueda, H., Iwai, A., Kuwako, K., Hori, M.E., 2006. Impact of anthropogenic forcing on the Asian summer monsoon as simulated by eight GCMs. Geophys. Res. Lett. 33, n/a-n/a. https://doi.org/10.1029/2005GL025336

Wang, B., 2005. Global Monsoon System : Research and Forecast. WMO Rep. 1266, 0–552.

Wang, B., Wu, Z., Li, J., Liu, J., Chang, C.-P., Ding, Y., Wu, G., 2008. How to Measure the Strength of the East Asian Summer Monsoon. J. Clim. 21, 4449–4463. https://doi.org/10.1175/2008JCLI2183.1

559 Wang, L., Chen, W., 2013. An Intensity Index for the East Asian Winter Monsoon. J. Clim. 27, 2361–
560 2374. https://doi.org/10.1175/JCLI-D-13-00086.1
561 Webster, P.J., Magaña, V.O., Palmer, T.N., Shukla, J., Tomas, R. a., Yanai, M., Yasunari, T., 1998.
562 Monsoons: Processes, predictability, and the prospects for prediction. J. Geophys. Res. 103,
563 14451. https://doi.org/10.1029/97JC02719
564 Webster, P.J., Yang, S., 1992. Monsoon and ENSO:Selectively interactive systems. Quart. J. Roy.
565 Meteorol. Soc. 118, 877–926.
566 Zhuang, G., Hourigan, J.K., Koch, P.L., Ritts, B.D., Kent-Corson, M.L., 2011. Isotopic constraints on
567 intensified aridity in Central Asia around 12Ma. Earth Planet. Sci. Lett. 312, 152–163.
568 https://doi.org/10.1016/j.epsl.2011.10.005
569